




RESEARCH ARTICLE | MARCH 21 2016

Dynamics of a reconnection-driven runaway ion tail in a reversed field pinch plasma **FREE**

J. K. Anderson ; J. Kim; P. J. Bonofiglio ; W. Capecchi; S. Eilerman ; M. D. Nornberg ; J. S. Sarff; S. H. Sears



Phys. Plasmas 23, 055702 (2016)

<https://doi.org/10.1063/1.4943525>

 CHORUS



Articles You May Be Interested In

Runaway of energetic test ions in a toroidal plasma

Phys. Plasmas (February 2015)

Fokker-Planck simulation of runaway electron generation in disruptions with the hot-tail effect

Phys. Plasmas (June 2016)

Hot tail runaway electron generation in tokamak disruptions

Phys. Plasmas (July 2008)



Physics of Plasmas

Special Topics Open
for Submissions

[Learn More](#)

Dynamics of a reconnection-driven runaway ion tail in a reversed field pinch plasma

J. K. Anderson,^{a),b)} J. Kim, P. J. Bonofiglio, W. Capecchi, S. Eilerman,^{c)} M. D. Nornberg, J. S. Sarff, and S. H. Sears

Department of Physics, University of Wisconsin-Madison, Madison, Wisconsin 53706, USA

(Received 30 November 2015; accepted 2 February 2016; published online 21 March 2016)

While reconnection-driven ion heating is common in laboratory and astrophysical plasmas, the underlying mechanisms for converting magnetic to kinetic energy remain not fully understood. Reversed field pinch discharges are often characterized by rapid ion heating during impulsive reconnection, generating an ion distribution with an enhanced bulk temperature, mainly perpendicular to magnetic field. In the Madison Symmetric Torus, a subset of discharges with the strongest reconnection events develop a very anisotropic, high energy tail parallel to magnetic field in addition to bulk perpendicular heating, which produces a fusion neutron flux orders of magnitude higher than that expected from a Maxwellian distribution. Here, we demonstrate that two factors in addition to a perpendicular bulk heating mechanism must be considered to explain this distribution. First, ion runaway can occur in the strong parallel-to-B electric field induced by a rapid equilibrium change triggered by reconnection-based relaxation; this effect is particularly strong on perpendicularly heated ions which experience a reduced frictional drag relative to bulk ions. Second, the confinement of ions varies dramatically as a function of velocity. Whereas thermal ions are governed by stochastic diffusion along tearing-altered field lines (and radial diffusion increases with parallel speed), sufficiently energetic ions are well confined, only weakly affected by a stochastic magnetic field. High energy ions traveling mainly in the direction of toroidal plasma current are nearly classically confined, while counter-propagating ions experience an intermediate confinement, greater than that of thermal ions but significantly less than classical expectations. The details of ion confinement tend to reinforce the asymmetric drive of the parallel electric field, resulting in a very asymmetric, anisotropic distribution. © 2016 AIP Publishing LLC.

[<http://dx.doi.org/10.1063/1.4943525>]

INTRODUCTION

Non-collisional heating and energization of ions is a powerful process in many astrophysical settings, such as the solar corona¹ and in laboratory plasmas including spheromak^{2,3} and reversed field pinch (RFP)^{4–9} plasmas. Particle runaway, where the presence of an electric field in excess of the frictional drag on the particle,¹⁰ is a candidate for an underlying mechanism of converting magnetic to kinetic energy. Runaway electrons, whose drag decreases monotonically with energy,¹¹ are well studied in tokamak fusion plasmas, where a disruption-induced runaway electron beam¹² could potentially damage next generation tokamak experiments. The frictional drag on an ion in a neutral Maxwellian plasma is non-monotonic, as it experiences a local maximum in Coulomb interactions at a speed near the ion thermal speed, and a second maximum at much higher energy near the electron thermal speed.

Runaway ions, like runaway electrons, are important in both the astrophysical and fusion laboratory settings. The abundance of high energy ions in solar flares, as an example,

is often attributed to runaway.¹³ The possibility of ion runaway in a toroidal pinch experiment dates back to the ZETA device.¹⁴ The conditions for runaway of a test ion in a tokamak plasma were set out by Furth and Rutherford through a solution of the ion drift kinetic equation,¹⁵ and runaway ions were observed in the MAST device driven by electric fields induced by internal reconnection events.¹⁶ High energy hydrogen ions ($40 - 80 \times T_i$) sourced by a neutral beam into a deuterium RFP plasma obey the test particle runaway model with an electric field induced by a global reconnection event.¹⁷ Recent computational work¹⁸ demonstrates the importance of collisional diffusion of runaway ions by comparison of Fokker-Planck calculations with test particle equations; this mandates going beyond test particle theory for explanation of ion dynamics in the RFP.

Ion runaway is intricately entwined with the non-collisional heating and energization of ions in the Madison Symmetric Torus (MST). Tearing activity (including linearly and nonlinearly driven modes which span the plasma column) saturates through dynamo-like feedback on the current density profile, rapidly releasing magnetic energy and inducing a strong impulsive, parallel-to-B electric field as poloidal magnetic flux is converted to toroidal flux.¹⁹ The global reconnection leads to strong ion heating in the MST where previous measurements detail a known anisotropy in temperature ($T_\perp > T_\parallel$)^{20–22} suggestive of a perpendicular bulk

Note: Paper DI2 2, Bull. Am. Phys. Soc. **60**, 107 (2015).

^{a)}Invited speaker.

^{b)}jkanders@wisc.edu

^{c)}Present affiliation: National Oceanic and Atmospheric Administration, Boulder, Colorado 80305, USA.

heating mechanism. In the subset of strongest reconnection events, multiple mechanisms combine to create a most interesting ion distribution. Runaway of the reduced-friction naturally heated ions generates an asymmetric ion tail with $E_{\parallel} \gg E_{\perp}$. The tail is reinforced by a confinement asymmetry, where runaway ions approach the limit of classical cross-field transport despite magnetic stochasticity from the broad spectrum of tearing modes. Confinement is lower in other regions of the v_{\perp}/v_{\parallel} plane and reduces to Rechester-Rosenbluth-like transport experienced by thermal particles.^{23,24}

Experiments with neutral beam injection elegantly confirm the ion runaway process¹⁷ and fast ion confinement characteristics in MST.^{25–27} Neutral particle analyzers measure parallel acceleration of the test particle distribution with the peak electric field exceeding the maximum ion-electron friction during the reconnection event. The energy gain is larger for higher initial ion energy (reduced drag), and deceleration is observed with reversed electric field (counter-current injection) according to runaway dynamics and confirmed with Fokker-Planck modeling. Full orbit test particle tracing in the 3D time evolving \mathbf{E} and \mathbf{B} fields (from visco-resistive MHD simulations)²⁸ corroborates the understanding of fast ion confinement.

In this work, we examine the high energy deuterium ion distribution generated naturally by global magnetic reconnection events in the MST. Measurement of the high energy ion distribution through three slices of velocity phase space demonstrates the need to consider two processes beyond the perpendicular bulk heating. Ion runaway in the inductive electric field accompanying self organization of the current profile is a key to generating the highest energy particles, while large variation of ion confinement times across velocity space reinforces a very asymmetric, anisotropic runaway ion distribution. It is shown that the runaway process is much more effective due to perpendicular heating of the bulk ions, resulting in a substantial population with reduced collisionality.

The energization reported here is due to global effects triggered by reconnection occurring simultaneously at many locations within the plasma column. We do not compare to models of direct energization of a particle in the fields of a single reconnecting layer as one might do to describe phenomena in the magnetosphere or dedicated laboratory reconnection experiments.²⁹ The focus of this work is on ion, not electron, dynamics; the accumulated ion distribution following several bursts of global reconnection results from a dramatic step change in particle confinement with energy. Bulk electrons, which respond quickly to an applied electric field, experience no such change in their confining properties, and acceleration along the stochastic magnetic field is equal to a sharp loss of confinement. While electron runaway is unlikely to be an important process in the RFP, studies of emission from an energized electron distribution in MST are the topic of future work.

SELF ORGANIZATION IN THE RFP

The RFP is conceptually a simple device: a strong current driven in a toroidal plasma column surrounded by a

conducting shell. The configuration is defined by a very high plasma current relative to magnetic field strength (around an order of magnitude higher than a tokamak) leading to a self-organized state where plasma currents generate nearly the entire confining magnetic field. The MST³⁰ ($R/a = 1.5$ m/0.52 m) operates with a plasma current between 200 and 600 kA, a core field strength of 0.2–0.6 T, a line averaged electron and deuteron density typically less than 2×10^{13} cm⁻³, central electron and ion temperatures of 200–2000 eV with a Lundquist number $S \sim 10^7$ and $\beta \sim 5\% - 10\%$ in the experiments considered here.

The relatively weak toroidal magnetic field makes the RFP susceptible to a number of low order tearing modes. The equilibrium fields in the MST device³¹ generate a monotonically decreasing safety factor profile with $q(0) \leq 0.2$ and a set of resonant tearing modes with poloidal mode number $m = 1$ and toroidal mode number $n \geq 6$. There is a surface where the toroidal component of magnetic field is zero and poloidally symmetric ($m = 0$) modes with any n are resonant; while linearly stable, a large $n = 1$ mode is often nonlinearly driven.

The strong drive of toroidal current is aligned with the magnetic field in the core, which steepens the parallel current density gradient and eventually drives a core mode unstable. There is rapid growth, and nonlinear transfer of energy to higher n through the $m = 0$ mode. These dynamics are illustrated in Figure 1, where a 500 kA MST discharge shows several strong, periodic sawtooth relaxations. These are identified by step-like increases in toroidal magnetic flux accompanying sharp bursts of magnetic fluctuations. The core-most resonant tearing mode ($n = 6$) is driven linearly unstable by ∇J_{\parallel} ; the $m = 1, n = 7$ and $m = 0, n = 1$ amplitudes demonstrate the importance of nonlinear drive and energy transfer.

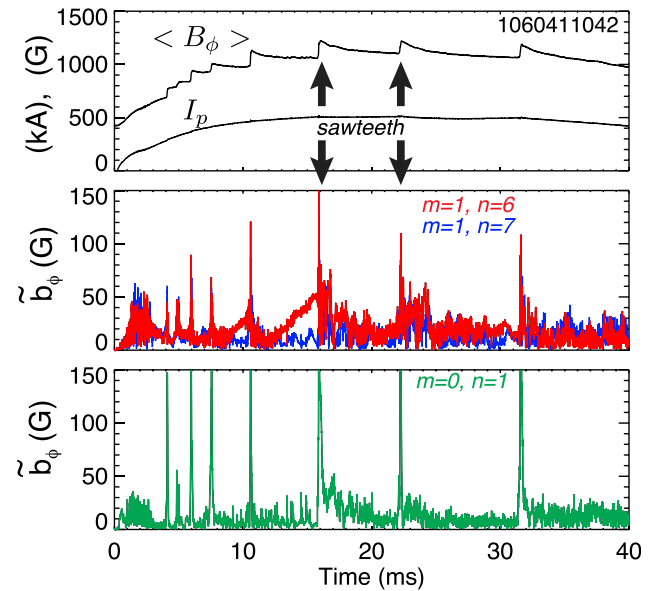


FIG. 1. (a) Plasma current and toroidal flux ($\Phi = \langle B_{\phi} \rangle \pi a^2$) within an RFP plasma are plotted. Sawteeth, identified as step-like increases in toroidal flux accompany bursts of magnetic fluctuations, both in core-resonant modes (b) and linearly stable, but nonlinearly driven, edge-resonant modes (c). Ion heating is well documented at these relaxation events.

Fluctuation based dynamo-like terms in a parallel Ohm's law $E_{\parallel} + \langle \tilde{v} \times \tilde{b} \rangle_{\parallel} - \frac{\langle \tilde{j} \times \tilde{b} \rangle_{\parallel}}{en} = \eta J_{\parallel}$ are substantial during periods of high tearing activity and provide a nonlinear reaction to the current profile. Here, the MHD and Hall dynamo terms have been measured as important contributors in MST plasmas.^{32,33} The resulting relaxation leads to a flatter current profile and a state more stable to tearing. The re-organization is shown in Figure 2(a) with a J_{\parallel} that is reduced in the core and increased at high radius; this is responsible for the step-like increase in toroidal magnetic flux but an overall decrease in stored magnetic energy. A substantial fraction of the lost magnetic energy is converted to ion heat, mainly perpendicular to the magnetic field, as has been well reported in the past, see Refs. 22 and 34 and references therein.

As the relaxation process takes about $100 \mu\text{s}$, there is a substantial induced electric field. A series of discrete equilibrium reconstructions specifies the magnetic field profiles as a function of time, and application of Faraday's law computes the electric field. The core value of the component parallel to magnetic field is plotted versus time in Figure 2(b). For perspective, note that the a time-averaged value of $E_{\parallel}(0)$ away from a sawtooth stays near 1 V/m . The impulsive electric field has a large effect on the resultant ion distribution, but perhaps more subtle is the effect of variation of ion confinement as a function of velocity.

CONFINEMENT OF IONS IN THE RFP

The radial magnetic field perturbations associated with the tearing modes govern thermal confinement in the RFP.²³ A substantial overlap of magnetic islands can occur and as such, the magnetic field in the RFP is typically stochastic. Rechester-Rosenbluth-like transport³⁵ limits electron and thermal ion confinement times to around 1 ms .

The confinement of fast ions is relatively insensitive to the stochastic field of the RFP. Despite the weak toroidal field and multiple resonant tearing modes which could diminish fast ion confinement,^{36,37} fast ions are observed to slow classically and have a confinement time much larger than thermal particles.²⁶ The dearth of transport within the modestly stochastic magnetic field is understood to result

from the decoupling of the fast ion orbits from the magnetic perturbations. In the RFP, with a magnetic field strongest at the magnetic axis and a dominant poloidal field over much of the minor radius, the drift-altered fast ion guiding center remains on a flux surface. Although well confined, the guiding center can wander and islands can develop in the ion guiding center motion analogous to magnetic islands on the field lines. The ions are routinely confined for up to a classical slowing time.²⁵

A neutral beam injector optimized for MST (with an accelerating voltage of $15\text{--}25 \text{ kV}$) is used to measure fast ion confinement and probe energetic ion physics. Complementing the NBI, a high energy neutral particle analyzer (NPA)^{38,39} is available to measure the distribution of high energy hydrogen and deuterium ions escaping the plasma via charge exchange. Ten energy-resolved channels measure particles of each species from 5 to 40 keV in energy, well above the thermal particle range of up to 2 keV . These are both instrumental in confirming ion runaway in MST.

The decay of neutron flux after turn-off of a short beam pulse of deuterium injection (the beam-blip technique⁴⁰) is used to infer the confinement of the fast ions, τ_{fi} . In the example in Figure 3(a), the neutron flux shown in red is measured for beam injection of ions parallel to the toroidal plasma current. The flux ramps up while NBI is on, and decays quite slowly at turn-off. A comparison between the measured neutron decay and that expected from classical slowing alone (perfect fast ion confinement) gives the computed fast ion confinement time. In this example, the computed time is approximately 13 ms .

A detailed τ_{fi} measurement over a range of stochasticity (and hence collisionality, by the strong effect on electron temperature) is presented in Ref. 26. It is important to note that the beam blip technique keeps the total fast ion content small, and the possibly destabilizing effects of a large fast ion population are not relevant. Over a large range of MST operating space, the confinement of fast particles is much better than thermal, and (within the sizable error bars of a neutral density measurement) consistent with the loss rate expected for charge exchange with a background neutral and subsequent loss of the energetic neutral.

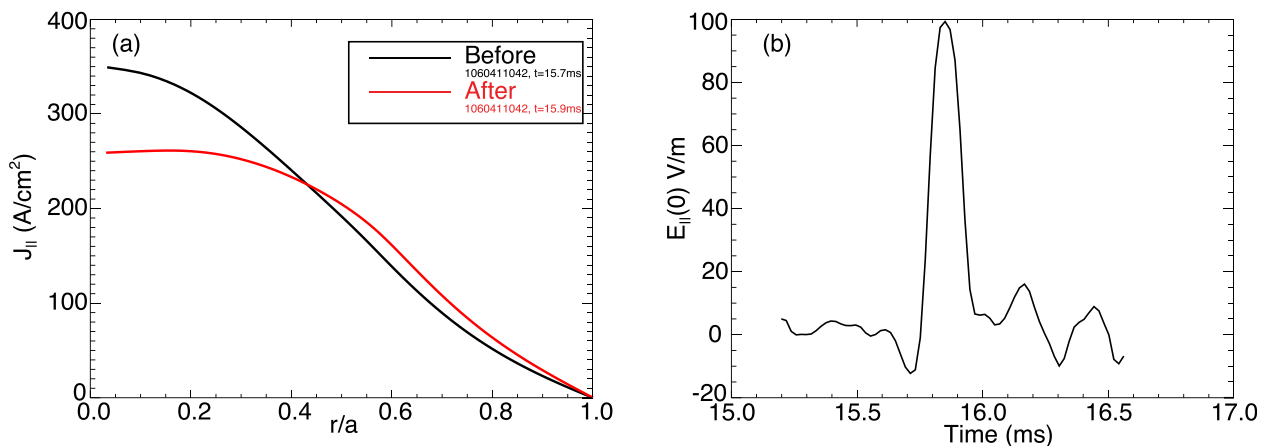


FIG. 2. (a) Parallel current density (J_{\parallel}) is plotted before and after sawtooth relaxation, demonstrating a reduced gradient and improved stability to tearing. In (b), the core value of field-aligned impulsive electric field induced by the rapidly changing magnetic field is plotted.

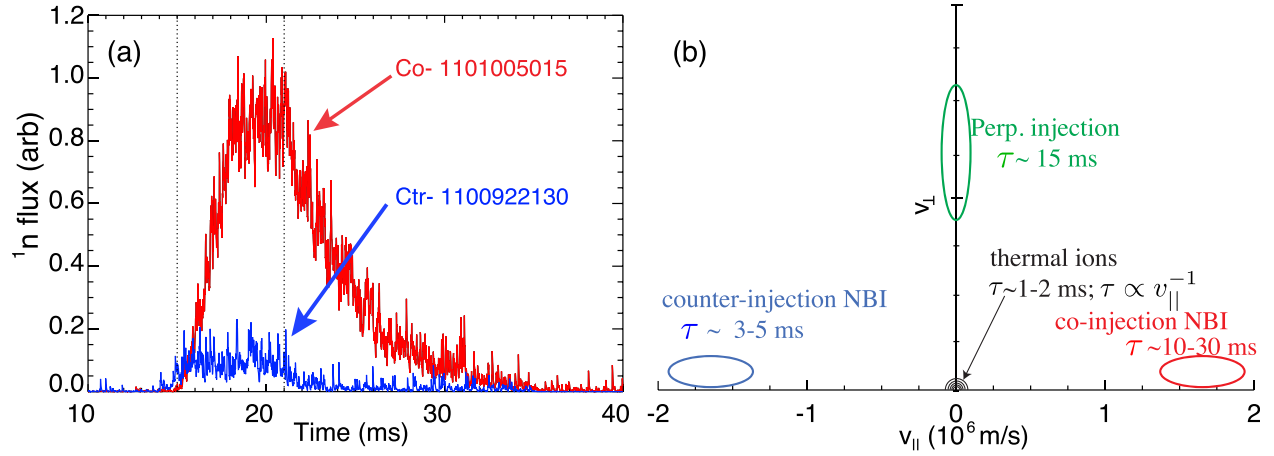


FIG. 3. (a) NBI-sourced test ions show a confinement asymmetry. In red, 25 keV D+ ions injected parallel to plasma current are well confined, with the example here resulting in a computed $\tau_{fi} \sim 13$ ms. In blue, D+ ions injected anti-parallel to plasma current have a much lower confinement. Typical fits in these discharges yield $\tau_{fi} \sim 3 - 5$ ms. (b) Illustration of known ion confinement behavior as a function of position in the v_{\perp}/v_{\parallel} plane. A boundary between thermal and highly energetic ions must exist. Ion confinement varies dramatically as a function of velocity.

The same technique applied for neutral beam injecting against plasma current (by reversing the direction of plasma current) confirms a much lower confinement. The neutron flux plotted in blue in Figure 3(a) is a representative example; the overall flux is much lower than co-injection (due to a combination of higher prompt loss and lower confinement), and the flux decay at beam turnoff is considerably faster than classical slowing would predict. Fitting typically yields fast ion confinement times of 3–5 ms for counter- I_p traveling ions in these plasma conditions.

Figure 3(b) is a consolidation of core-localized ion confinement as a function of position in the v_{\perp}/v_{\parallel} plane in MST; there is a strong variation. While this graph illustrates asymmetry in $v_{\parallel} = \frac{\mathbf{v} \cdot \mathbf{B}}{|\mathbf{B}|}$ with respect to core magnetic field, the important physics lie with the direction of plasma current (and hence B_{θ}). The radial component of the Lorentz force from $v_{\phi} B_{\theta}$ creates the asymmetry between co- and counter- I_p passing fast ions. In addition to the two tangential NBI measurements, previous work on MST utilized a neutral beam mounted radially,⁴¹ injecting perpendicular to the magnetic field. Here, the ∇B contribution dominates the guiding center drift of the fast ions and there is again a substantial deviation from the magnetic field lines; much better than thermal confinement is observed. Interestingly, thermal particles (near the origin) are least-well confined as motion along the stochastic field lines governs cross-field transport. Typical confinement times are on the order of a millisecond, and the confinement is expected to decrease with parallel speed. Clearly there exists a critical energy along the $v_{\perp} = 0$ axis where a transition in confinement occurs; it remains to be found experimentally as it is below the operating range of the injector. The confinement variation plays an important role in the development of the observed runaway distribution.

ION RUNAWAY IN THE REVERSED FIELD PINCH

Figure 4 is an example discharge affected by natural ion runaway. Current just over 500 kA is plotted along with $m = 0$ magnetic fluctuations (Figure 4(a)) to mark the times

of impulsive reconnection. In Figure 4(b), ion temperature from two diagnostics (one measuring a carbon impurity,⁴² the other the bulk deuterium⁴³) is plotted; both measure temperature by sampling the distribution perpendicular to the magnetic field. There is a measurable D-D fusion neutron flux (black line in Figure 4(c)) which exceeds the expected flux computed using a Maxwellian distribution at the measured temperature (blue line) by several orders of magnitude. The large discrepancy requires further consideration of the distribution. The idea of a runaway ion tail (parallel to B, to which these T_i diagnostics are not sensitive) has been previously suggested,^{14,44} and recently the runaway process has been clearly identified in lower current discharges in MST.¹⁷

The sawtooth-induced equilibrium change generates a toroidally symmetric parallel electric field which can overcome the drag of classical Coulomb collisions as shown in Figure 5(a). The frictional force on a test ion (from bulk

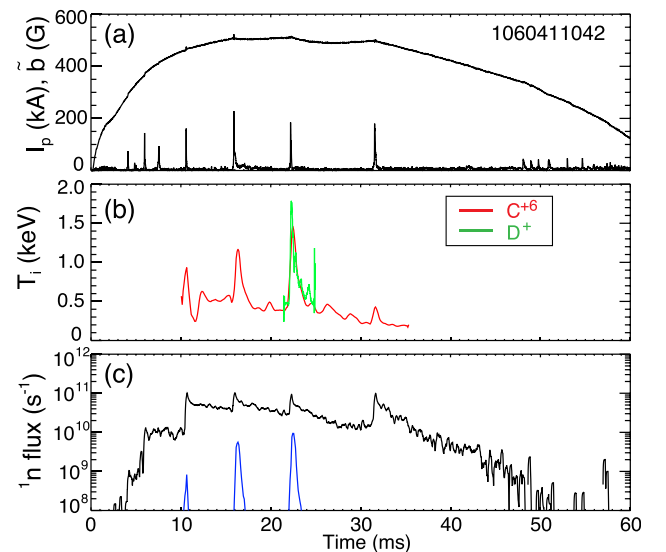


FIG. 4. Plasma current and magnetic fluctuations (a) in a 500 kA MST discharge, clearly identify time points where measured ion temperature (b) (impurity and bulk) is enhanced. The measured neutron flux (c) (black line) dramatically exceeds that expected for a thermal distribution (blue line).

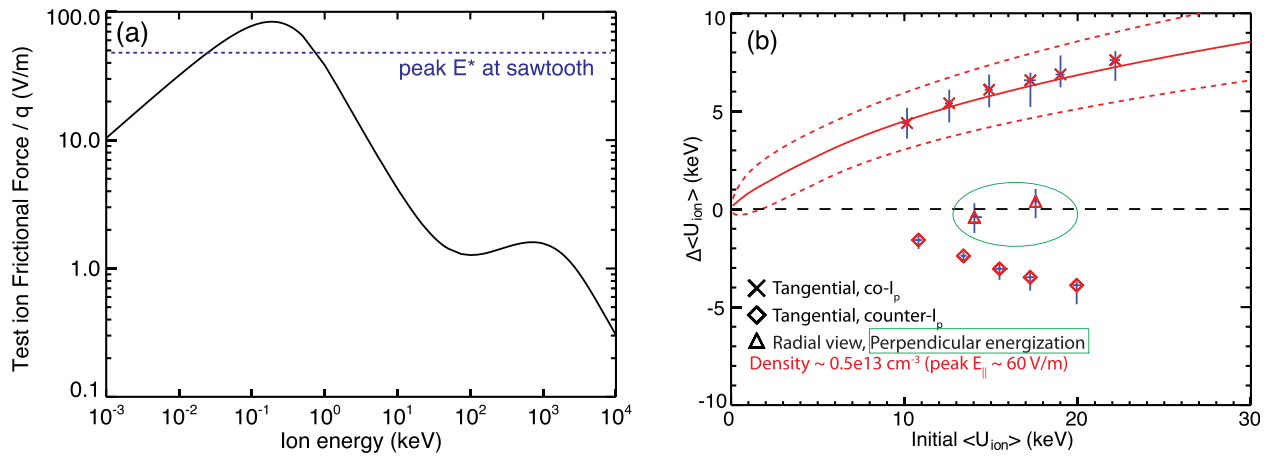


FIG. 5. (a) Friction on test ion due to Coulomb collisions; ions with above 1 keV of energy are accelerated for a significant portion of the 100 μ s sawtooth field. (b) Runaway of test ions is confirmed by varying initial energy through neutral beam injection. (Similar to figure in Ref. 17). It is important to note that the data match the simple model for ion runaway, which shows very small energy gain for thermal (<1 keV) ions. Additionally, the perpendicular energy gain is measured to be zero for fast test ions.

electron density and temperature measurements) is plotted as a function of ion energy. Following the Furth and Rutherford analysis,¹⁵ the electric field is properly corrected, $E^* = E \left(1 - \frac{Z}{Z_{eff}}\right) f\left(\frac{n_e^r}{n_e}\right)$ as interaction with drifting electrons acts to cancel a portion of the accelerating electric field. In a pure, homogeneous plasma the cancellation is complete, but in these MST discharges, $E^*/E \simeq 80\%$ is computed through a spatial average over the plasma core where the fast ions are localized. There is an estimated $Z_{eff} \simeq 4$ due to finite impurity content and a modest trapped particle fraction due to toroidal geometry; a sensitivity study⁴⁵ shows the approximate 80% fraction is robust to the assumptions made.

The strength of E^* at the sawtooth crash is indicated for plasma conditions used in test particle studies in Figure 5(b). The test particle studies are conducted in lower plasma current discharges (with lower impulsive electric fields) relative to the discharges with a strong naturally occurring runaway population (e.g., Figure 4). The electric field computed in Figure 2(b) is representative of the high current discharges and is used in the Fokker-Planck modeling, while the test particle experiments have typical peak value of $E_{||} \sim 60$ V/m. Away from the sawtooth, the electric field is generally about 1 V/m—insufficient to overcome drag.

The quantitative identification of ion runaway used the NBI to fast hydrogen within the deuterium plasma. A fast turn-off of the NBI at a sawtooth removes the rapid sourcing of particles at the injection energy, enabling a clean calculation of the change in average energy of the NPA-measured test particle distribution. Figure 5(b) contains many measurements, each averaged over many similar sawteeth for several beam energies, and three distinct NPA views.

In the default view, the NPA samples core-localized ions traveling nearly parallel to the toroidal plasma current. The second view is achieved by reversal of the toroidal plasma current and the NPA-sampled ions are traveling against I_p (and against the strong impulsive electric field accompanying the burst of reconnection). Finally, relocation of the NPA from a tangentially viewing port to a radial

viewing port directs it to sample ions with a high perpendicular energy.

In the parallel-to- I_p view (\times plot symbols in Figure 5(b)), a clear energy gain is observed at a sawtooth with peak $E_{||} \sim 60$ V/m. These studies are performed at a comparatively modest set of plasma parameters in MST, with plasma current 300 kA, central electron density of 5×10^{12} cm $^{-3}$, and electron temperature of about 300 eV. The beam injection energy is scanned, revealing the energy gain increases with initial energy. A simple test particle model computes the expected runaway energy gain as a function of initial energy, computed for injection parallel to I_p , and is plotted as the solid red line in Figure 5(b). The error bars (dotted lines) are estimated from an uncertainty in electron temperature and effective ionic charge of the plasmas. The model matches the measurements very well.

In the case of inverted plasma current, the sawtooth-driven electric field opposes the motion of the test ions and substantial deceleration is observed (\diamond plot symbols in Figure 5(b)). An expected energy change is not plotted, as the finite confinement time of counter-injected ions invalidates the extremely simple model. The measurements, though, show a clear deceleration, precluding processes such as Fermi acceleration where $\Delta U \propto U^{1/2}$ could be expected. Finally, with a perpendicular viewing NPA, 15–18 keV test particles (\triangle plot symbols in Figure 5(b)) are not measurably energized by the reconnection process.

RECONNECTION-DRIVEN RUNAWAY ION TAIL

In the highest current MST discharges illustrated in Figures 1, 2, and 4, the fusion neutron flux far exceeds the expectation from thermal ions. Ion runaway and the details of ion confinement are both key contributors to the generation of this distribution. Figure 6 is a set of measurements of the core-localized hot distribution on three views through velocity phase space: (a) anti-parallel to toroidal plasma current (I_p), (b) perpendicular to the core current and magnetic field, and (c) parallel to I_p . The top panel of each is the measured neutron flux as a function of time, which shows a

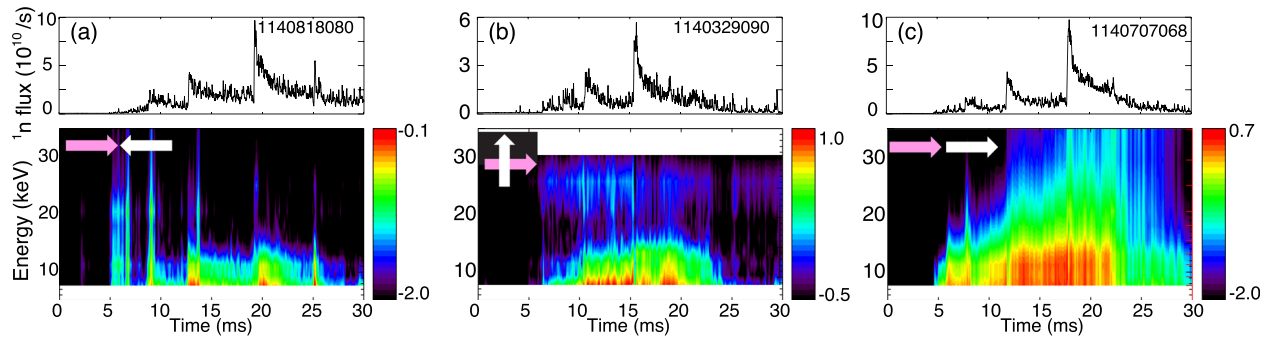


FIG. 6. Three NPA views sample the fast deuterium distribution. In (a), the particles traveling against plasma current are measured. An uptick is observed at each reconnection event, and a finite confinement is evident by the loss of particles between sawteeth. In (b), the diagnostic collects particles with energy perpendicular to magnetic field. Here (well above thermal energies), a hot population develops, is well confined (based on the steady signal between sawteeth), but once established, is not further energized where large increases in fusion neutron flux are observed. In (c), particles traveling along the plasma current are measured; a well-confined, high energy distribution is measured.

discrete step at each reconnection event. Simultaneous measurement of the three views is not possible due to hardware limitations, so many reproducible discharges are studied. These three are representative of the high neutron flux producing discharges. The NPA-measured fast ion distribution is the contour plot in the lower panel of each, and includes a pair of arrows to indicate the direction of measured particles (white) relative to plasma current (pink). Spatial localization of the line-of-sight-averaged neutral particle analysis is notoriously tricky,⁴⁶ however, the three views mentioned here are unique in their sampling of the plasma core; all sample low pitch ions originating from higher radius. The stark differences in the three observations confirm the assumption of measurement of core-localized ions.

Comparison of parallel to perpendicular reveals a strong anisotropy. The parallel-to- I_p energetic ions (Figure 6(c)) show a high energy tail, developed in discrete steps, with substantial particle count at energies above 30 keV. Between the energization events, the steady particle flux is indicative of good confinement of these high $v_{||}$ ions. The perpendicular view (Figure 6(b)), where a temperature increase is expected at the reconnection event (based on many past measurements) shows a population that grows in energy to approximately 12 keV and stabilizes. Good confinement of these ions is surmised between events due to the nearly constant 10–12 keV NPA signals in the absence of a source. Of particular interest, note that the perpendicular distribution is not significantly altered at $t = 15$ ms, where the neutron rate jumps sharply due to a strong reconnection event.

In addition to the anisotropy, there is an extremely strong asymmetry in the $v_{\perp} \sim 0$ ions. Figure 6(a) is a sample of particles traveling against the plasma current. Relative to co- I_p (Figure 6(c)), there is clearly a smaller particle flux and the number of high energy particles steadily decreases following a burst. The evolution of the distribution is affected by confinement, which tends to reinforce the asymmetry from one-directional field-aligned drive at the sawtooth.

The CQL3D code,⁴⁷ a Fokker-Planck solver well suited for the toroidal RFP magnetic geometry, evolves the ion distribution through the time-dependent inductive parallel electric field and qualitatively matches experimental observations. A general species of deuterium ions is modeled through three

background Maxwellian species (deuterium ions, electrons, and fully stripped aluminum, whose density is specified to match the estimated core $Z_{eff} \simeq 4$). The energetic ion distribution resulting from a balance between collisions, the dc electric field, and radial diffusion is calculated as a function of radius and two velocity coordinates, employing bounce averaging. In these simulations, the collision operator is fully non-linear and includes interactions with both the general and Maxwellian species, and radiation losses are neglected. A primary limitation on modeling herein is that radial diffusion is not enhanced above classical diffusion. This description is sufficient for the high pitch, high energy ions, but is inadequate in modeling the physics of thermal and counter-propagating ions. As such, quantitative comparison with the experimental neutron flux or NPA distribution measurements is not valid, although the modeling does show that a perpendicular heating of the bulk prior to (or simultaneous with) the parallel electric field makes a substantial difference in the runaway population.

A two-step heating process is suggested and illustrated in Figure 7. A 500 eV Maxwellian ion distribution, Figure 7(a), has a perpendicular heating applied to raise the perpendicular temperature to about 1500 eV, Figure 7(b). In practice, this is achieved by setting up a non-equilibrium initial distribution roughly in agreement with anisotropic impurity temperature measurements immediately following a burst of reconnection in MST.²² This distribution is subjected to the impulsive parallel electric field, Figure 7(c), resulting in the asymmetric runaway distribution in Figure 7(d). The modeled electric field is chosen to mimic experimental conditions, an impulsive burst of amplitude $E^* = 0.8E_{||}(0) = 80$ V/m lasts 100 μ s, with the time axis defined $t = 0$ at instant of peak electric field, and returns to the between-sawtooth value of 1 V/m.

The change in distribution function (Figure 7(e)) and expected fusion neutron production (Figure 7(f)) is compared for the two cases. Black lines indicate the Maxwellian initial distribution and red lines the pre-heated distribution. Two separate simulations (not shown) are used to plot the expected neutron flux as a function of time. The first applies the parallel electric field to the Maxwellian distribution, black curve in Figure 7(f). The second evolves the

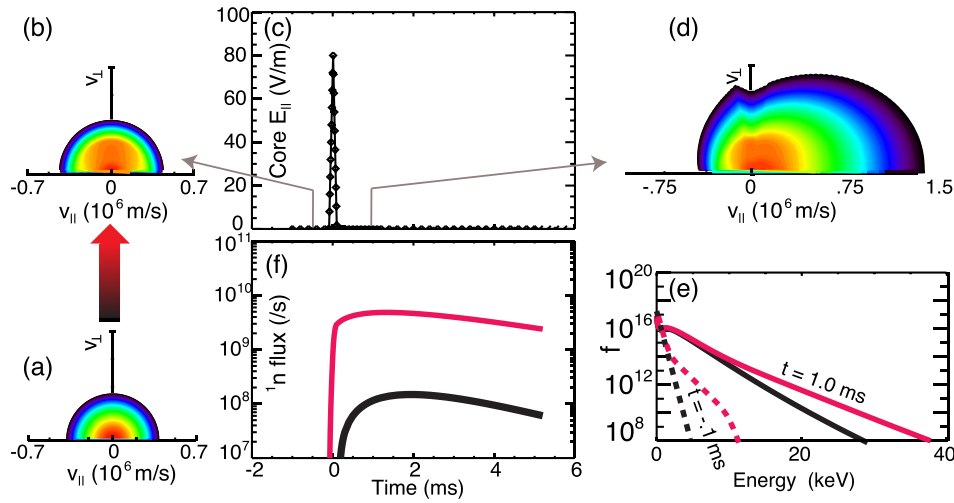


FIG. 7. A two-step heating process is suggested. A 500 eV Maxwellian ion distribution (a) is altered to raise the perpendicular temperature to about 1500 eV (b). This distribution is subjected to the impulsive parallel electric field (c), resulting in the asymmetric runaway distribution (d). A separate simulation (not shown) applies the parallel electric field to the Maxwellian distribution. The change in distribution function (e) and expected fusion neutron production (f) is compared for the two cases. Black lines indicate the Maxwellian initial distribution and red lines the pre-heated distribution. The reduced collisionality of the pre-heated distribution leads to a notable difference in distribution function above 10 keV and a substantially higher neutron flux.

pre-heated distribution in time without a sawtooth electric field; the red curve in Figure 7(f) subtracts these baseline neutrons to isolate the effect of the impulsive field on the preheated distribution. Energy gain through the runaway process is small for thermal ions. The reduced collisionality of the pre-heated distribution leads to a notable difference in distribution function above 10 keV and a substantially higher (more than an order of magnitude) neutron flux.

Some simple comparisons between the single-sawtooth simulations and experimental measurements can be made, although in experiment multiple sawteeth occur, spaced far enough apart in time that the differing confinement time-scales play a major role. The high pitch (parallel to I_p) ions are well confined, most susceptible to subsequent acceleration, and accumulate. Near-thermal ions can be an important contributor to the total neutron flux as they are abundant, but with confinement falling with $v_{||}$ until sufficient energy is reached for improved confinement, the quick loss could account for the sharp drop of neutron rate immediately following a burst as seen in Figure 4(c). After the brief initial decay, a longer timescale of neutron flux is evident, likely from the fusion of well-confined high energy ions. The distributions calculated from the Fokker-Planck analysis can be qualitatively compared with the NPA measurements, although neither an absolute calibration nor a parallel- to perpendicular-line-of-sight relative calibration is available. The distribution following the electric field burst in the simulation roughly maps to the three NPA views where Figure 6(a) is a line of $v_{||} < 0$ at $v_{\perp} = 0$; Figure 6(b) is the $v_{||} = 0$ axis, and Figure 6(c) is $v_{||} > 0$ at $v_{\perp} = 0$. Similarity is apparent insofar as a large affect is observed at high $v_{||}$, a large asymmetry exists between $v_{||} < 0$ and $v_{||} > 0$, and the modest change in the distribution at $v_{||} = 0$. The simulations show tail acceleration for about a millisecond following the impulsive reconnection as the between-sawtooth electric field can exceed friction for the highest energy particles.

Although the details of the perpendicular heating mechanism(s) are not critical to this work (where an ad hoc initial distribution is specified), in light of the new observations it seems relevant to recall a stochastic heating mechanism proposed by Fiksel *et al.* in 2009.²¹ Radial motion of ions through stochastic diffusion coupled with strong radial electric field fluctuations from tearing modes heats particles perpendicular to B . With reasonable values of D_{\perp} , \bar{E}_r , and a radial correlation length of the tearing fluctuations, the theory matches the intense observed heating rate, the mass dependence, and several other phenomena, but notably misses the generation of a fast tail to very high energy. The runaway process is shown here to be quite capable of further modification of the distribution.

Two new observations suggest the dominant perpendicular heating mechanism is ineffective on high energy particles, possibly linked to the crossing of a boundary in phase space from stochastic confinement to near classical confinement of sufficiently energetic ions. At high enough energy, the perpendicular ions are well-confined in the stochastic field ($D_{\perp} \rightarrow 0$), and the proposed stochastic heating mechanism shuts off. This agrees with the careful runaway test ion measurements, where dominantly perpendicular ions were not further energized. It also is consistent with the distribution measurements in the naturally occurring runaway distribution shown here: the perpendicular distribution is heated to the point where a healthy population of 10–15 keV ions exists (and based on time dependence are well confined), but with subsequent violent reconnection events that dramatically increase the neutron flux, there is not a substantial change in the perpendicular distribution.

The stochastic mechanism is not the only suggested theory for perpendicular heating observations, but is worthy of mention here due to the mechanism's need for high radial diffusivity to efficiently heat ions. These two observations with low D_{\perp} due to improved confinement show minimal, if any, perpendicular heating at the reconnection event.

SUMMARY

The observation and study of a naturally occurring ion distribution, which produces 2–3 orders of magnitude more fusion neutrons than expected from a thermal distribution alone, uncovers some physics behind the energization of ions in the RFP. We suggest a two-step process where stochastic heating, perpendicular to magnetic field, makes conducive the parallel runaway of a substantial number of ions. Dramatic variation of ion confinement as a function of velocity contributes strongly to the developed ion distribution.

Ions are heated perpendicular to the magnetic field at the reconnection event, according to numerous observations over the years with a host of possible explanations. Two features in present observations of the non-thermal ion distribution corroborate a stochastic heating mechanism. While the parallel energy discretely steps up from one reconnection event to the next, the distribution of dominantly perpendicular high energy particles remains relatively unchanged. These ions are, indeed, well-confined, as the population holds steady between impulsive energization events. Test particle methodology shows no perpendicular energy gain of test ions at such an event. These are both suggestive of a perpendicular heating mechanism that diminishes as the confinement changes from very diffusive to very well confined.

This stochastic mechanism, where radially diffusing ions on stochastic field lines are influenced by radial electric field perturbations, phenomenologically matches several features of perpendicular ion heating in MST, but notably misses the generation of a parallel tail. Recent work confirmed ion runaway of NBI-sourced fast test particles, which are both well confined and at reduced collisionality when compared to thermal ions. The perpendicularly heated ions also satisfy the criteria to runaway in the sawtooth electric field.

Regardless of the perpendicular heating mechanism invoked, both ion runaway and the confinement variation are crucial in development of the observed distribution. Fokker-Planck modeling demonstrates that raising the perpendicular temperature by about a factor of three leads to a substantial population of ions in a range where the runaway mechanism can add significant energy. Runaway of a perpendicularly heated ion distribution generates a tail which has a fusion rate more than an order of magnitude above that of a Maxwellian distribution subjected to the impulsive electric field. Ongoing work will incorporate the ion confinement characteristics into Fokker-Planck modeling and may improve the time dependence of the expected neutron flux.

Notably absent in this work is any mention of electron energization. The large inductive electric fields considered here would presumably cause runaway of electrons as well as ions, however there is no indication that confinement of electrons in the stochastic field would transition away from the Rechester-Rosenbluth mechanism. An electron accelerated parallel to magnetic field will be quite poorly confined, particularly at the time of peak applied electric field due to large radial magnetic field perturbations. Deduction of an energetic electron distribution by measure of x radiation is a

topic of current investigation on MST; forthcoming analysis will help formulate the more general understanding of reconnection-driven particle energization in MST. Data shown in this paper can be obtained in digital format.⁴⁸

ACKNOWLEDGMENTS

This material is based upon work supported by the U.S. Department of Energy Office of Science, Office of Fusion Energy Sciences program under Award No. DE-FC02-05ER54814. Portions of the work were accomplished with the use of infrastructure of Complex DOL (BINP, Russia).

- ¹E. R. Priest, C. R. Foley, J. Heyvaerts, T. D. Arber, J. L. Culhane, and L. W. Acton, *Nature* **393**, 545 (1998).
- ²Y. Ono, M. Yamada, T. Akao, T. Tajima, and R. Matsumoto, *Phys. Rev. Lett.* **76**, 3328 (1996).
- ³M. R. Brown, C. D. Cothran, M. Landreman, D. Schlossberg, W. H. Matthaeus, G. Qin, V. S. Lukin, and T. Gray, *Phys. Plasmas* **9**, 2077 (2002).
- ⁴B. Jones and R. Wilson, *Nucl. Fusion Suppl.* **3**, 889 (1962).
- ⁵R. B. Howell and H. J. Karr, *Phys. Fluids* **19**, 2012 (1976).
- ⁶G. A. Wurden, P. G. Weber, K. F. Schoenberg, A. E. Schofield, J. A. Phillips, C. P. Munson, G. Miller, J. C. Ingraham, R. B. Howell, J. N. Downing, and Others, in *Proceedings of the 15th European Conference on Controlled Fusion and Plasma Physics*, Technical Report (Los Alamos National Lab., NM, USA, Dubrovnik, 1988).
- ⁷A. Fujisawa, H. Ji, K. Yamagishi, S. Shinohara, H. Toyama, and K. Miyamoto, *Nucl. Fusion* **31**, 1443 (1991).
- ⁸E. Scime, S. Hokin, N. Mattor, and C. Watts, *Phys. Rev. Lett.* **68**, 2165 (1992).
- ⁹P. Hörling, G. Hedin, J. H. Brzozowski, E. Tennfors, and S. Mazur, *Plasma Phys. Controlled Fusion* **38**, 1725 (1996).
- ¹⁰H. Dreicer, *Phys. Rev.* **115**, 238 (1959).
- ¹¹R. M. Kulsrud, Y.-C. Sun, N. K. Winsor, and H. A. Fallon, *Phys. Rev. Lett.* **31**, 690 (1973).
- ¹²E. M. Hollmann, N. Commaux, N. W. Eidietis, T. E. Evans, D. A. Humphreys, A. N. James, T. C. Jernigan, P. B. Parks, E. J. Strait, J. C. Wesley *et al.*, *Phys. Plasmas* **17**, 056117 (2010).
- ¹³G. D. Holman, *Astrophys. J.* **452**, 451 (1995).
- ¹⁴A. Gibson, *Nature* **183**, 101 (1959).
- ¹⁵H. P. Furth and P. H. Rutherford, *Phys. Rev. Lett.* **28**, 545 (1972).
- ¹⁶P. Helander, L.-G. Eriksson, R. Akers, C. Byrom, C. Gimblett, and M. Tournianski, *Phys. Rev. Lett.* **89**, 235002 (2002).
- ¹⁷S. Eilerman, J. K. Anderson, J. S. Sarff, C. B. Forest, J. A. Reusch, M. D. Nornberg, and J. Kim, *Phys. Plasmas* **22**, 020702 (2015).
- ¹⁸O. Embréus, S. Newton, A. Stahl, E. Hirvijoki, and T. Fülöp, *Phys. Plasmas* **22**, 052122 (2015).
- ¹⁹H. A. B. Bodin and A. A. Newton, *Nucl. Fusion* **20**, 1255 (1980).
- ²⁰S. T. A. Gangadhara, D. Craig, D. A. Ennis, D. J. Den Hartog, G. Fiksel, and S. C. Prager, *Phys. Rev. Lett.* **98**, 075001 (2007).
- ²¹G. Fiksel, A. F. Almagri, B. E. Chapman, V. V. Mirnov, Y. Ren, J. S. Sarff, and P. W. Terry, *Phys. Rev. Lett.* **103**, 145002 (2009).
- ²²R. M. Magee, D. J. Den Hartog, S. T. A. Kumar, A. F. Almagri, B. E. Chapman, G. Fiksel, V. V. Mirnov, E. D. Mezonlin, and J. B. Titus, *Phys. Rev. Lett.* **107**, 065005 (2011).
- ²³T. M. Biewer, C. B. Forest, J. K. Anderson, G. Fiksel, B. Hudson, S. C. Prager, J. S. Sarff, J. C. Wright, D. L. Brower, W. Ding, and S. Terry, *Phys. Rev. Lett.* **91**, 045004 (2003).
- ²⁴G. Fiksel, A. F. Almagri, J. K. Anderson, A. D. Beklemishev, B. E. Chapman, D. Craig, V. I. Davydenko, D. J. Den Hartog, D. Ennis, S. Gangadhara *et al.*, in *21st IAEA Fusion Energy Conference* (Chengdu, 2006).
- ²⁵G. Fiksel, B. Hudson, D. J. Den Hartog, R. M. Magee, R. O'Connell, S. C. Prager, A. Beklemishev, V. I. Davydenko, A. A. Ivanov, and Y. Tsidulko, *Phys. Rev. Lett.* **95**, 125001 (2005).
- ²⁶D. Liu, A. F. Almagri, J. K. Anderson, V. Belykh, B. E. Chapman, V. I. Davydenko, P. Deichuli, D. J. Den Hartog, S. Eilerman, G. Fiksel, C. B. Forest, A. A. Ivanov, M. D. Nornberg, S. V. Polosatkin, J. S. Sarff, N. Stupishin, and J. Waksman, in *38th EPS Conference on Plasma Physics* (Strasbourg, France, 2011), Vol. 35G, p. P2.101.

- ²⁷J. K. Anderson, W. Capecchi, S. Eilerman, J. J. Kollner, L. Lin, M. D. Nornberg, J. A. Reusch, and J. S. Sarff, *Plasma Phys. Controlled Fusion* **56**, 094006 (2014).
- ²⁸J. A. Reusch, J. K. Anderson, and Y. Tsidulko, *Nucl. Fusion* **54**, 104007 (2014).
- ²⁹M. Yamada, J. Yoo, J. Jara-Almonte, W. Daughton, H. Ji, R. M. Kulsrud, and C. E. Myers, *Phys. Plasmas* **22**, 056501 (2015).
- ³⁰R. N. Dexter, D. W. Kerst, and T. W. Lovell, *Fusion Technol.* **19**, 131 (1991).
- ³¹J. K. Anderson, C. B. Forest, T. M. Biewer, J. S. Sarff, and J. C. Wright, *Nucl. Fusion* **44**, 162 (2004).
- ³²H. Ji, A. F. Almagri, S. C. Prager, and J. S. Sarff, *Phys. Rev. Lett.* **73**, 668 (1994).
- ³³W. X. Ding, D. L. Brower, D. Craig, B. H. Deng, G. Fiksel, V. V. Mirnov, S. C. Prager, J. S. Sarff, and V. Svidzinski, *Phys. Rev. Lett.* **93**, 045002 (2004).
- ³⁴M. S. Cartolano, D. Craig, D. J. Den Hartog, S. T. A. Kumar, and M. D. Nornberg, *Phys. Plasmas* **21**, 012510 (2014).
- ³⁵A. B. Rechester and M. N. Rosenbluth, *Phys. Rev. Lett.* **40**, 38 (1978).
- ³⁶H. E. Mynick, *Phys. Fluids B* **5**, 1471 (1993).
- ³⁷C. B. Forest, J. R. Ferron, T. Gianakon, R. W. Harvey, W. W. Heidbrink, A. W. Hyatt, R. J. La Haye, M. Murakami, P. A. Politzer, and H. E. S. John, *Phys. Rev. Lett.* **79**, 427 (1997).
- ³⁸S. V. Polosatkin, V. Belykh, V. I. Davydenko, R. Clary, G. Fiksel, A. Ivanov, V. Kapitonov, D. Liu, V. Mishagin, M. Tiunov, and R. Voskoboinikov, *Nucl. Instrum. Methods Phys. Res., Sect. A* **720**, 42 (2013).
- ³⁹J. A. Reusch, J. K. Anderson, V. Belykh, S. Eilerman, D. Liu, G. Fiksel, and S. V. Polosatkin, *Rev. Sci. Instrum.* **83**, 10D704 (2012).
- ⁴⁰W. W. Heidbrink, J. Kim, and R. J. Groebner, *Nucl. Fusion* **28**, 1897 (1988).
- ⁴¹B. Hudson, "Fast ion confinement in the reversed-field pinch," Ph.D. thesis (University of Wisconsin–Madison, 2006).
- ⁴²D. Craig, D. J. Den Hartog, G. Fiksel, V. I. Davydenko, and A. A. Ivanov, *Rev. Sci. Instrum.* **72**, 1008 (2001).
- ⁴³J. C. Reardon, G. Fiksel, C. B. Forest, A. F. Abdrashitov, V. I. Davydenko, A. A. Ivanov, S. A. Korepanov, S. V. Murachtin, and G. I. Shulzhenko, *Rev. Sci. Instrum.* **72**, 598 (2001).
- ⁴⁴R. M. Magee, "Ion energization during tearing mode magnetic reconnection in a high temperature plasma," Ph.D. thesis (University of Wisconsin–Madison, 2011).
- ⁴⁵S. Eilerman, "Ion runaway during magnetic reconnection in the reversed-field pinch," Ph.D. thesis (University of Wisconsin–Madison, 2014).
- ⁴⁶S. Eilerman, J. K. Anderson, J. A. Reusch, D. Liu, G. Fiksel, S. Polosatkin, and V. Belykh, *Rev. Sci. Instrum.* **83**, 10D302 (2012).
- ⁴⁷R. W. Harvey, in Summary of the IAEA Technical Committee Meeting on Advances in Simulation and Modeling of Thermonuclear Plasmas, Montreal, 1992; U.S. Department of Commerce, NTIS, Doc. No. DE93002962, 1992.
- ⁴⁸See supplementary material at <http://dx.doi.org/10.1063/1.4943525> for the digital format of the data shown in this paper.